ELSEVIER

Physica B 228 (1996) 1–10

PHYSICA B

Hydraulic jumps, flow separation and wave breaking: An experimental study

Tomas Bohr*, Clive Ellegaard, Adam Espe Hansen, Anders Haaning

Center for Chaos and Turbulence Studies, The Niels Bohr Institute, Blegdamsvej 17, 2100 Copenhagen Ø, Denmark

Abstract

We describe experimental results on the circular hydraulic jump in a viscous fluid (ethylene-glycol mixed with water) in a setup, where the depth of the fluid far away from the jet is controlled. On increasing the depth, we find a transition from a state (type 1) with separation occurring only on the bottom, to a state (type 2) with a "roller", i.e. separation occurring also on the free surface, as in a broken wave. The system is laminar both before and after the transition and can thus be very accurately controlled. We present data for the height profile of the fluid layer, for the surface velocity and for the location of the separation points. Further, we show direct numerical simulations of the Navier–Stokes equations confirming our interpretation of the transition.

Keywords: Hydraulic jumps; Flow separation; Wave breaking

1. Introduction

The circular hydraulic jump appears when a vertical fluid jet impinges on a horizontal surface. Under azimuthally symmetrical conditions, the flow is purely radial and independent of angle. Close to the jet the fluid layer is thin and the motion is rapid: further away it is an order of magnitude thicker and moves correspondingly slower. The transition between these two types of motion takes place in a surprisingly abrupt manner, i.e. in a narrow annular region, defining rather precisely a radius r_j, of the hydraulic jump. Photographs of hydraulic jumps under various conditions to be explained later, are shown on Fig. 1(a)–(d).

The hydraulic jump is well-known, at least in its more turbulent form, for most people experienced in dish washing. It has also been studied scientifically, although relevant references and, more importantly, genuine understanding of the phenomenon, is very sparse.

Hydraulic jumps occur also in channels and rivers, i.e. basically a 1–D setting. In this context the most famous appearance is the so-called "river bore", which occurs in rivers close to the outlet into a sea with strong tidal variations, when the tidal wave propagates up the river. Shallow water theory, which is mathematically equivalent to the equations for strongly compressible fluid flow (i.e. gas theory), predicts the occurrence of shocks, at which the height of the free surface and the mean fluid velocity are discontinuous. As in the case of gas flow, there has been a considerable controversy over the relevant jump conditions across such a discontinuity. The resolution proposed by Lord Rayleigh in 1914 [1] is now widely accepted: across the jump, fluid flux and momentum flux should be

*Corresponding author.

0921-4526/96/$15.00
PII S0921-4526(96)00373-0

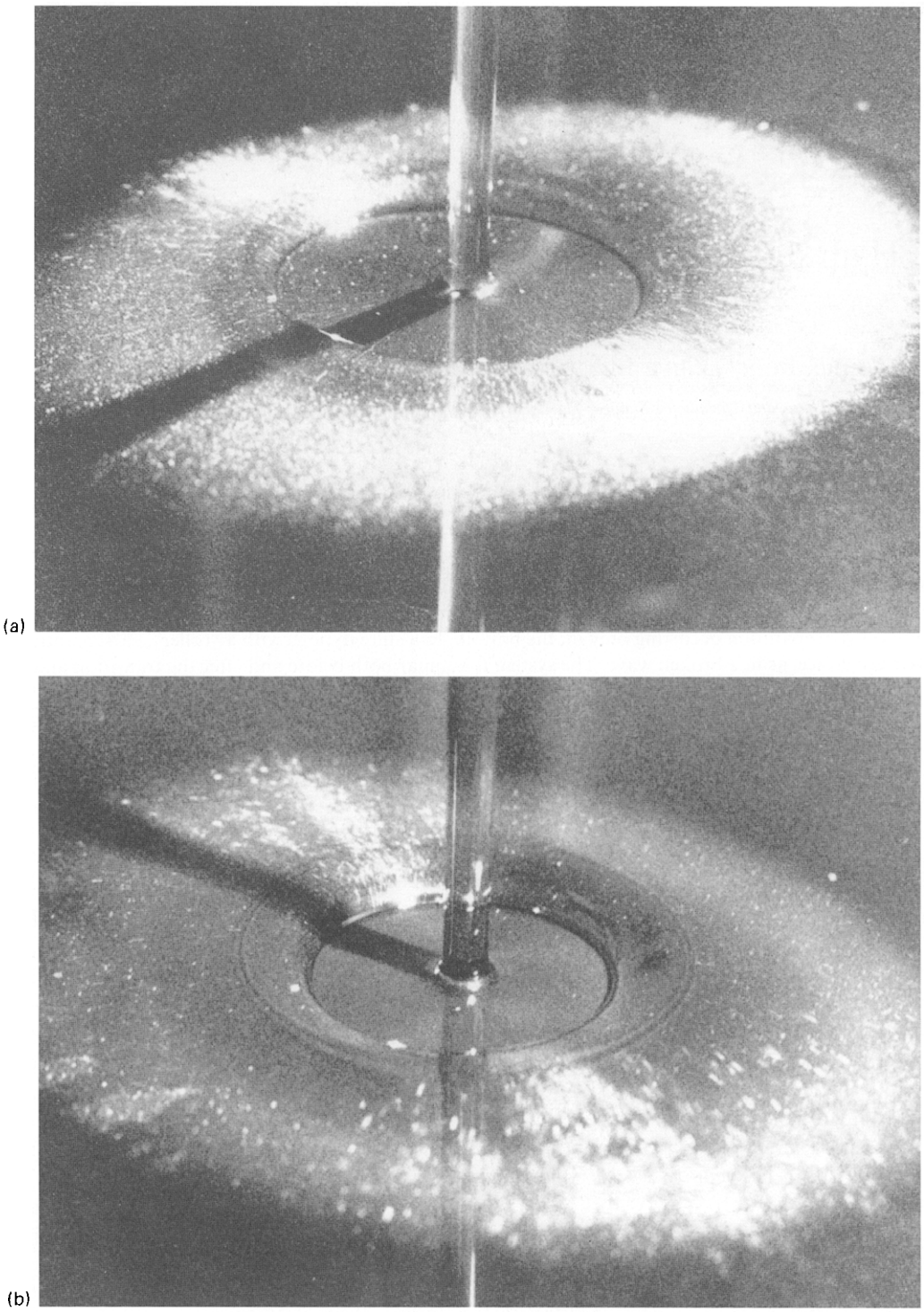

Fig. 1. Photos of the circular hydraulic jump. See Section 3 for explanation of the classifications used below. The downstream depth is smallest at photo (a) and increasing with largest depth at (d). (a) Type 1 flow; (b) type 2 flow; (c) time-dependent flow with a hexagonal jump region; (d) flow with no (ordinary) jump.

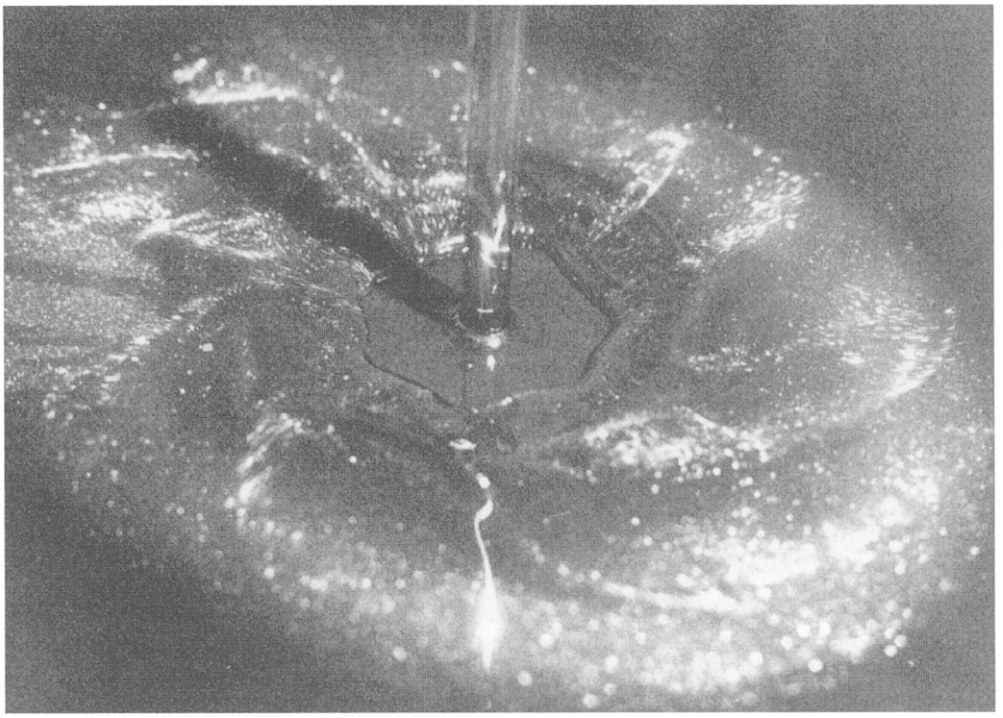

(c)

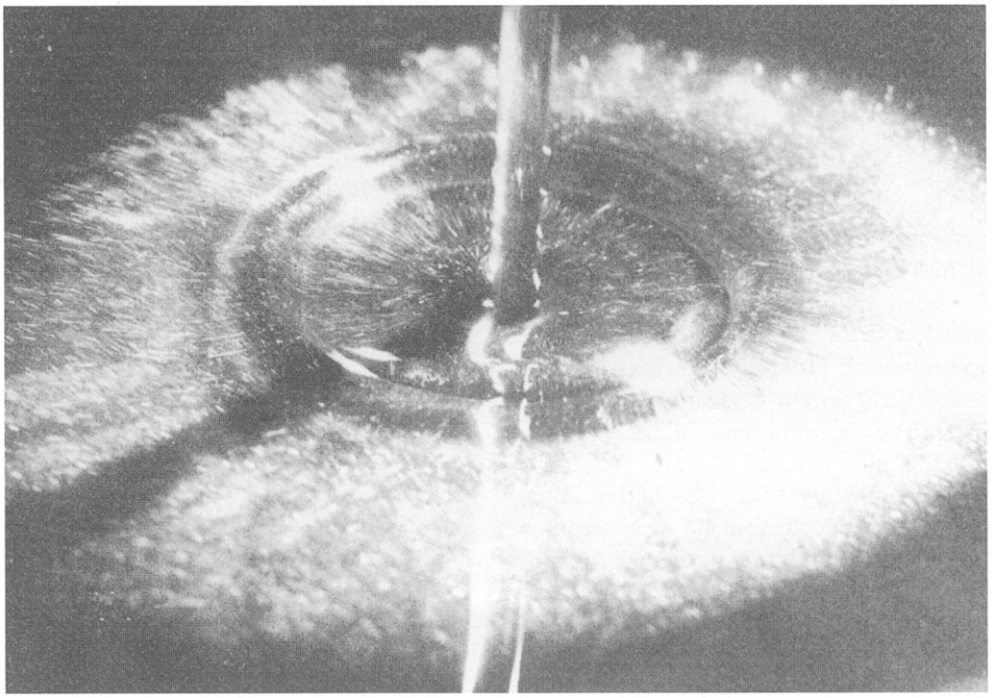

(d)

Fig. 1. Continued

conserved, but not energy flux. The reason for the lack of energy conservation is ascribed to excitations in degrees of freedom, which are not properly taken into account by shallow water theory, and by viscous effects in the jump region.

A closer look at hydraulic jumps in the linear and radial cases, confirms Lord Rayleigh's criteria at least roughly [2], but also reveals that the structure of the flow is rather complicated [3, 4]. First of all, the jump seems invariably accompained by *separation*. i.e. the occurrence of regions with backflow. Separation can even happen in the form of a "roller". i.e. like the top of a broken wave. In the 1-D version, hydraulic jumps are basically always turbulent. This is not so in the radial case. With careful control of the jet and the right choice of fluid, the circular hydraulic jump can be kept laminar, even in the case containing a roller. This allows precise and reproducible measurements of phenomena closely akin to wave breaking. At higher flow rates the system eventually reaches a turbulent state.

Lord Rayleigh's shock conditions imply that the fluid before and after the jump are, respectively, "supercritical" and "subcritical", which means that the average velocity is, respectively, larger and smaller than the velocity of small amplitude waves, $\sqrt{gh}$. But this does not lead to a prediction of the location of the jump, if nothing further is known about, say the rate of energy dissipation [5]. In a homogenuos channel, a "hydraulic jump" will, in general, move, since there is nothing to keep it in place. The radial jump is stationary and the origin of the jump has to be sought in the fact that the layer, because of the radial spread, becomes very thin and the shear forces correspondingly large, which leads to separation. Thus a better understanding of this phenomenon and the instabilities occurring will hopefully lead to a better understanding of separation phenomena in general and thus to a better understanding of the onset of turbulence in the vicinity of rigid (and free) surfaces.

2. Experimental setup

The experimental setup is shown in Fig. 2. The fluid flows down from a container out of the nozzle

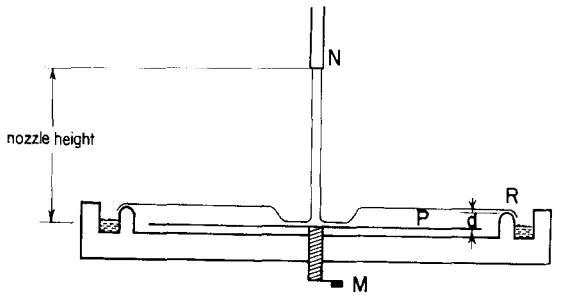

Fig. 2. Experimental setup: (N) is the nozzle, (P) the plate, (R) the rim (or weir), and (M) a handle by which the plate can be moved vertically, and thus d can be varied. Vertical fluid height is exaggerated.

(N). The free jet impinges on the circular plate (P), which can be moved in the vertical direction by turning the handle (M). The fluid passes a circular fixed rim (R), and is recycled to the container via a pump ensuring constant flux out of N. By moving the plate, the height difference d from the bottom of the plate to the top of the rim, and hence the external height H of the fluid layer, can be varied.

The fluid is ethylene-glucol (anti-freeze) mixed with water in the approximate ratio 4:1 and seeded with Iridion pearl lustre powder for visualization. The kinematic viscosity ν is 10–14 times that of water (i.e. $(1.0\text{–}1.4)\times 10^{-5}$ m^2/s). The flow is very dependent on viscosity, tending to be unstable if ν is lowered. The density is 1.11 kg/l and the surface tension is 4.5×10^{-2} N/m.

The distance from the nozzle to the plate was typically 11 cm, but the flow does not show any strong dependence on this parameter.

The fluid flux Q can be varied by regulating the outflow from the tank. It was typically 0.03 l/s. With a fluid height h, a mean velocity u and a radius r, the Reynolds number can be defined as

$$R = \frac{uh}{\nu} = \frac{Q}{2\pi\nu\tau} \tag{1}$$

since $Q = 2\pi ruh$. Typical values of the jump radius r_j were 2 cm, so the corresponding Reynolds number is of the order

$$R \approx \frac{0.03\times 10^{-3}}{2\pi\times 0.02\times 10^{-5}} \approx 25. \tag{2}$$

The height of the fluid layer is measured by a needle pointing vertically downward. Two step-motors allow it to be moved in the radial and horizontal directions. It is stepped down in the vertical direction until (electric) contact is made with the fluid surface and returns back up when the height has been registered. It is then stepped in the radial direction until the entire height profile is measured.

Separation phenomena are measured visually, either by observing the powder already present in the fluid, or by adding small amounts near the bottom and observing the direction of transport. The jump position and the positions of separation, both at the bottom and at the surface, are measured accurately with the help of a telescope.

Surface velocities are observed by monitoring small flakes of white paint dropped on the surface. The movement of the flakes is recorded photographically using a strobe-light with a well-known frequency.

3. Experimental results

The flow structure and thus the radius of the hydraulic jump depends strongly on flow rate and viscosity. For the case where the outer fluid falls freely over the edge of the plate (corresponding to $d \approx 0$) the jump-radius has been found to scale roughly as [5]

$$r_j = Q^{5/8} \nu^{-3/8} g^{-1/8}. \tag{3}$$

The corresponding flow is the one shown in Fig. 1(a).

We now present results showing the qualitative changes in the flow structure that occur as d is increased from zero, and the downstream height H gets correspondingly larger than the "free" value.

In Fig. 3 we show a series of measured height profiles for varying d but fixed flow rate Q. The lowest profile corresponds to $d = 0$, where the fluid flows freely from the plate. As d is increased the jump steepens and the jump radius r_j diminishes until the profile marked I, where an abrupt transition occurs. Suddenly the jump region becomes wider and the flow structure changes dramatically. On further increasing d, the fluid remains

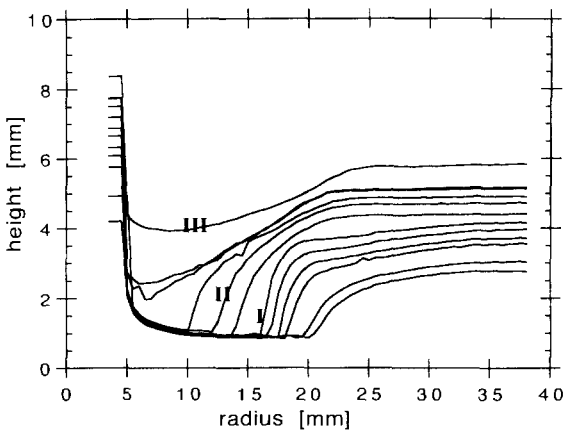

Fig. 3. Height profiles for varying d. The lowest profile corresponds to $d = 0$. I marks the last type 1 profile, just before the transition to type 2 flow. II marks the transition to unstable flow. III marks the situation where the jump has disappeared.

in this state until the profile marked II, where jump starts to vibrate. Later on the flow couples to the angle variable, i.e. becomes nonaxisymmetric, and time dependent, which is reflected in the irregularities of the profiles. Eventually r_j (which is now rather ill-defined), is of the order of the jet radius, and the jump disappears, as seen on the profile III.

In the time-dependent regime, before the jump disappears, the jump typically forms a polygon, instead of a circle. Often it has a hexagonal shape, as shown on the photograph Fig. 1(c). There are fast jets of fluid from the corners, and the whole structure is rotating. For constant d in this regime, we observe arbitrary shifts between direction of rotation of the hexagon, and less symmetric shapes. When the jump has disappeared, the height of the fluid is nowhere very small. On the other hand, as shown in Fig. 1(d), a "virtual" jump is still present in the flow.

Up to the profile marked II, the flow is stationary, and axisymmetric. We will from now on focus on this situation, and in particular on the transition mentioned above.

The transition at I is very well-defined, reversible and as far as we can see, no hysteresis occurs. We shall call the state corresponding to small H "type 1" and the state at large H, "type 2".

By observing the particles in the flow, we see that the transition from type 1 to type 2 induces a major

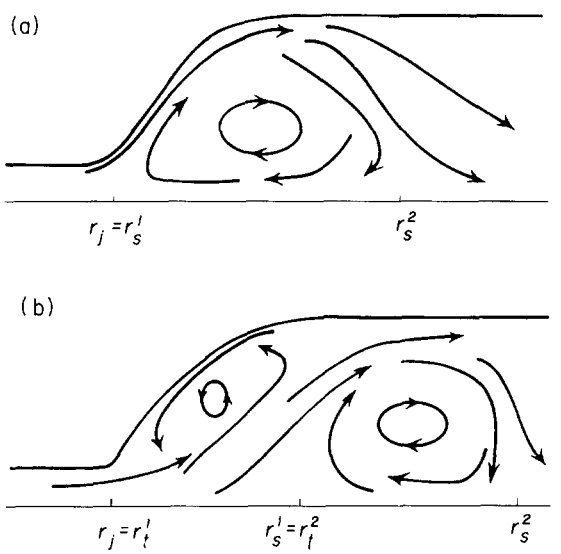

Fig. 4. Sketch of streamlines for (a) type 1 and (b) type 2 flow. The flow separates from the bottom at $r_s^{(1)}$, and reconnects at $r_s^{(2)}$. The roller at the fluid surface (for type 2 flow), lies between $r_t^{(1)}$ and $r_t^{(2)}$. Experimentally, $r_t^{(2)}$ cannot be distinguished from $r_s^{(1)}$.

restructuring of the flow. Figs. 4(a) and (b) shows our visual estimate for the streamlines in the two cases. Thus, the type 1 jump contains a separation "bubble" between points $r_s^{(1)}$, and $r_s^{(2)}$ in which reversed flow occurs. The surface moves forward at all points. In the type 2 case the surface velocity at the top is reversed in the jump region. A "roller" appears in the top layer between points $r_t^{(1)}$ and $r_t^{(2)}$, before the separation bubble. The surface velocity in the jump region can be very small in this state, and particles on the surface can be caught for a long time near r_j.

Fig. 1(a) shows a type 1 flow, and Fig. 1(b) shows a type 2 flow. In the latter case, the separation point $r_t^{(2)}$ on the surface is seen as a circular ring, whereas $r_t^{(1)}$ coincides with the jump.

In Fig. 5 we show the variation of some of the separation points with H. Thus, we plot the jump radius r_j and the reconnection points $r_t^{(2)}$ for the roller (only for type 2) and $r_s^{(2)}$ for the separation bubble. Note that $r_s^{(2)}$ is practically fixed and that $r_t^{(2)}$ remains close to the value of r_j for small H. The separation point $r_s^{(1)}$ is within the accuracy of our measurements, identical to $r_t^{(2)}$ and thus the entire separation bubble remains almost fixed while the jump moves and the structure changes.

The surface velocity measurements corresponding to type 1 is shown on Figs. 6(a) and (b). Fig. 6(a) shows the region before the jump including the jump region in which the velocity diminishes abruptly. Before the jump we see a regime of linearly

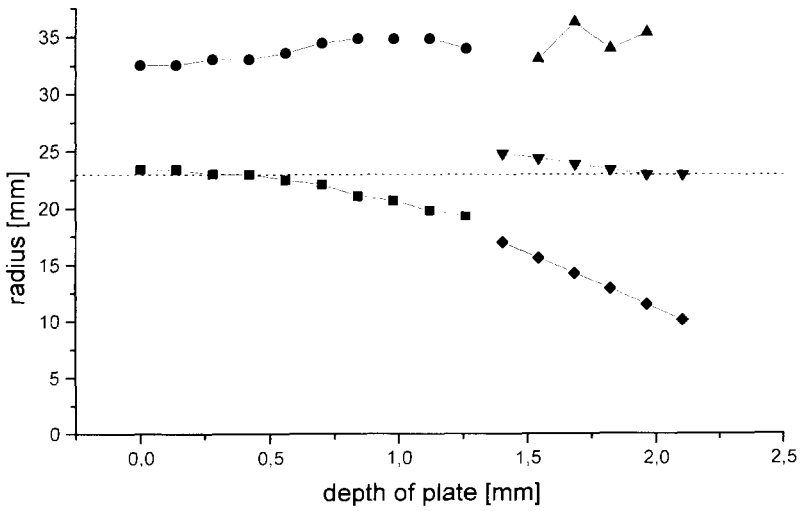

Fig. 5. Jump radius and separation points versus d. The transition from type 1 to type 2 flow happens as d is increased from 1.25 mm. Jump radius r_j is marked by squares before the transition and by diamonds after the transition, reconnection point for the separation bubble on the bottom $r_s^{(2)}$ by circles (before transition) and up triangles (after transition), and reconnection point for roller $r_t^{(2)}$ by down triangles (only for type 2). Experimental data: $Q = 0.031$ l/s, $\nu = 0.97 \times 10^{-5}$ m^2/s.

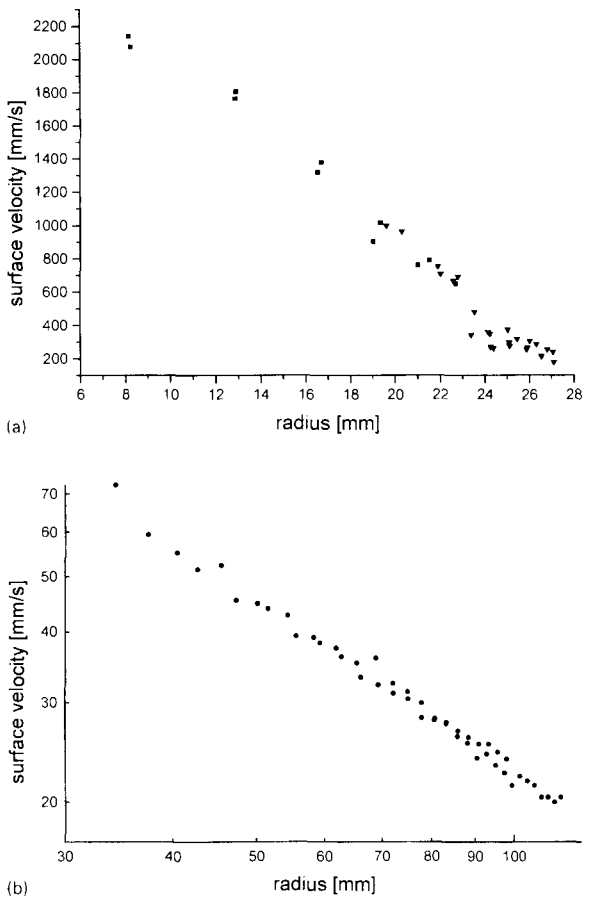

Fig. 6. Surface velocity in type 1 flow, for two regions. (a) Before and around the jump, which is located at $r = 24$ mm. Before the jump the velocity is decreasing linearly. At the jump the velocity diminishes abruptly. (b) After the jump. Log-log scale. Linear regression gives slope $= -0.99$, corresponding to the decay $v \sim 1/r$. Experimental data: $Q = 0.034$ l/s, $\nu = 14.4 \times 10^{-6}$ m^2/s, $d = 1.1$ mm.

decreasing surface velocity and after the jump (Fig. 6(b) we find that the surface velocity decays like $1/r$. Very similar behavior is found for the surface velocity in a type 2 jump: Before the jump the decay is linear and after the jump approximately as $1/r$.

4. Results of simulations

The theoretical description of the jump takes as starting point the full hydrodynamic equations (the Navier–Stokes equations) for a radially symmetric stationary state with a free surface. With the velocity radial velocity component u, vertical component w, pressure p and fluid height h, they are

$$uu_r + wu_z = -\frac{1}{\rho} p_r + \nu u_{zz} + \nu \left(u_{rr} + \frac{1}{r} u_r - \frac{1}{r^2} u \right), \tag{4}$$

$$uw_r + ww_z = -\frac{1}{\rho} p_z + \nu w_{zz} + \nu \left(w_{rr} + \frac{1}{r} w_r \right) - g, \tag{5}$$

where subscripts denote partial derivatives. The incompressibility condition is

$$u_r + \frac{u}{r} + w_z = 0 \tag{6}$$

and the boundary conditions at the free surface (neglecting surface tension) are

$$w(r, z = h) = u(r, z = h)h', \tag{7}$$

$$-(u_z + w_r)(1 - h'^2) - 2(w_z - u_r)h' = 0, \tag{8}$$

$$\frac{1}{\rho} p = 2\nu w_z - \nu(w_r + u_z)h' \tag{9}$$

and with no-slip condition on the bottom.

In order to by-pass the severe difficulties caused by the free surface, we have replaced it by a fixed, but stress-free surface with a given, prescribed shape in our simulations, i.e. we fix the surface and solve for the flow. The simplest choice is a piecewise linear surface with a shape close to the one we observe, and between this surface and the rigid bottom, we solve the Navier–Stokes equations by discretizing with second-order finite centered differences on a rectangular network of gridpoints. Then an iterative relaxation method is applied to find a stationary solution respecting the boundary conditions (7) and (8) as described e.g. in [8]. With our algorithm (i.e. fixing $h(r)$) it was not possible to fulfill Eq. (9) exactly, but large violations led to divergences and thus to no stationary state. This means that the chosen height profile must be reasonably close to the observed one.

As we are interested in the structure of the flow in the jump region, the simulation starts at a radius

r_1 somewhat less than the jump radius r_j, and ends at a radius r_2, 1.5–2.0 times r_j. With the chosen piecewise linear and fixed surface, we have the freedom of varying: the position of the jump, r_j; the slope h' of the surface in the jump region; the fluid height before (h_1) and after (h_2) the jump, and the velocity at r_1. The flow was not sensitive to the kind of velocity profile used at r_1, as long as the flux Q was kept constant. We used a parabolic profile for $u(r_1, z)$. At r_2 the velocities are set equal to their (left) neighbors, since we are in a region where there are no changes in the flow structure.

In Figs. 7(a) and (b) we show results of the simulations made for two different choices of r_j, h_1, h_2, h' and $u(r_1, h_1)$. Fig. 7(a) is a result with parameters chosen close to experimental data for a type 1 flow. The line shows the streamline connecting the separation points on the bottom (i.e. delimiting the separation bubble). Here the slope of the surface is $h' = 1.01$, corresponding to the maximum measured slope, which occurs just after r_j. On Fig. 7(b) parameters are chosen according to the experimental data for a type 2 flow. The slope has increased to $h' = 1.33$ (which is a bit larger than the measured $h' = 1.25$), and now the transition has occurred. The roller is marked on the top. The results of the simulations are remarkably close to the conjectured flow structures shown in Fig. 4.

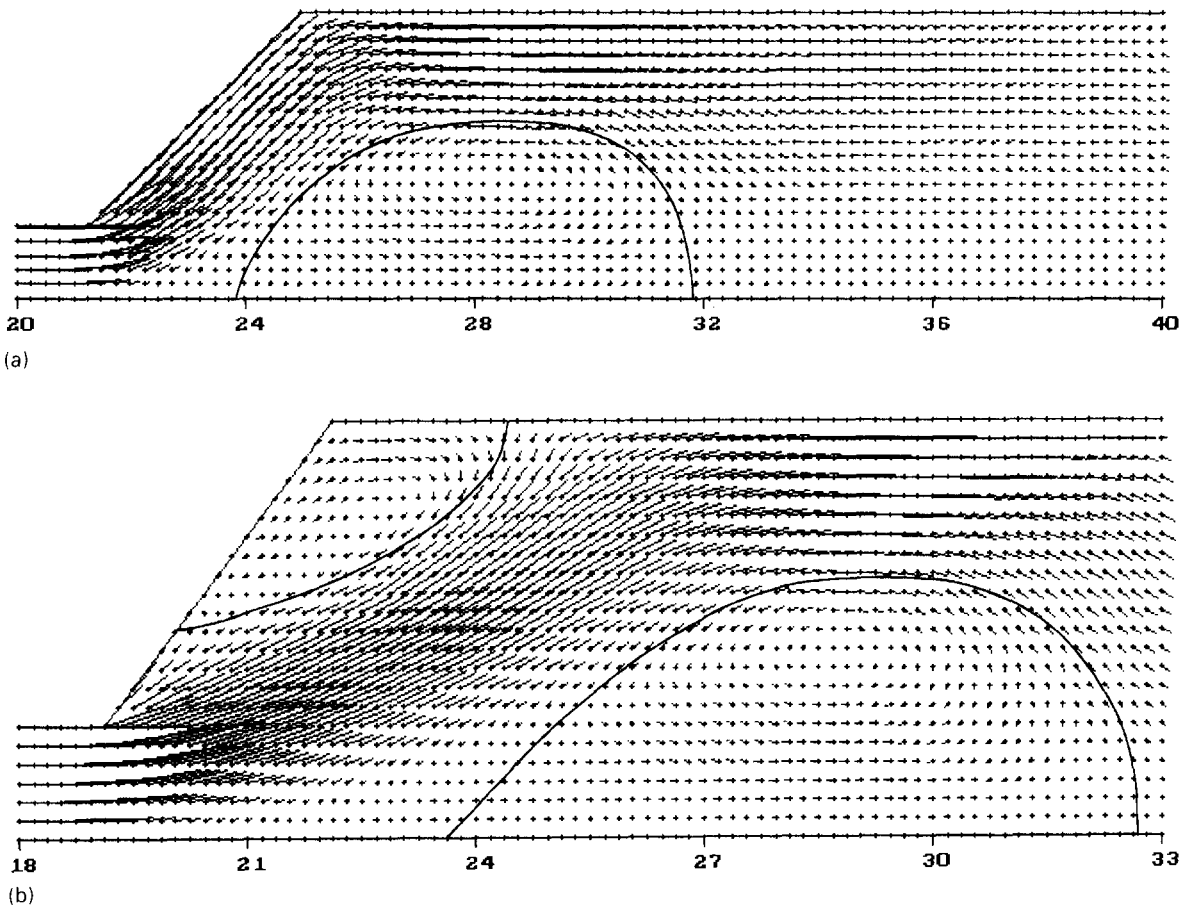

Fig. 7. Results of simulations for (a) type 1 and (b) type 2 flow. Units on the axes is mm. (a) Parameters are: Slope $h' = 1.01$, upstream height $h_1 = 1.25$ mm, downstream height $h_2 = 5.00$ mm, jump radius $r_j = 21.2$ mm, surface velocity (at $r = 20$ mm) $u(r_1, h_1) = 42$ cm/s. Note the separation bubble. (b) Parameters are: Slope $h' = 1.33$, upstream height $h_1 = 1.50$ mm, downstream height $h_2 = 5.5$ mm, jump radius $r_j = 19.3$ mm, surface velocity (at $r = 18$ mm) $u(r_1, h_1) = 49$ cm/s. Note the separation bubble and the roller at the surface.

We emphasize that our method is not self-consistent since the shape of the surface cannot be influenced by the flow. However, if we do not choose surface parameters close to the experimental data (for instance, if we take $u(r_1, h)$ too large), the simulation will generally diverge, as a result of the nonphysical conditions invoked.

5. Simplified theory

The standard way of describing a thin layer of fluid is by using Prandtl's boundary layer approximation corresponds to the assumption that vertical variations are much more rapid that radial ones. Thus we get

$$uu_r + wu_z = -\frac{1}{\rho} p_r + \nu u_{zz}, \tag{10}$$

$$0 = -\frac{1}{\rho} p_z - g. \tag{11}$$

In this approximation the boundary conditions (9) and (8) are simplified to

$$p(r, z = h) = 0, \tag{12}$$

$$u_z(r, z = h) = 0. \tag{13}$$

The vertical momentum equation together with Eq. (12) yields the hydrostatic pressure

$$p = \rho g(h - z) \tag{14}$$

and thus Eq. (10) becomes

$$uu_r + wu_z = -gh' + \nu u_{zz} \tag{15}$$

together with the incompressibility condition (6).

These equations can be made dimensionless [5] by the transformations

$$\begin{aligned} u &= a\tilde{u}, \quad a = q^{1/8}\nu^{1/8}g^{3/8}, \\ w &= b\tilde{w}, \quad b = q^{-1/4}\nu^{3/4}g^{1/4}, \\ r &= cx, \quad c = q^{5/8}\nu^{-3/8}g^{-1/8}, \\ z &= dy, \quad d = q^{1/4}\nu^{1/4}g^{-1/4}. \end{aligned} \tag{16}$$

Dropping the tilde, the rescaled equations are then

$$uu_x + wu_y = -h' + u_{yy}, \tag{17}$$

$$u_x + x^{-1}u + w_y = 0, \tag{18}$$

where, analogously, $h = d\tilde{h}$.

These equations will generically be singular at separation. It was shown already in 1948 by Goldstein [9] (for a standard boundary layer without a free surface) that, if the skin friction, which is proportional to $u_z(r, z = 0)$) goes through zero, it will generically happen in a square root singularity. This leads to a divergence of w, obviously in conflict with the assumptions of boundary layer theory. The same thing happens for in the free surface case. One way to see this is to assume that the velocity profile can be approximated by a low-order polynomial, say

$$u(x, y) = a(x)y + b(x)y^2 + c(x)y^3 + d(x)y^4. \tag{19}$$

Inserting this ansatz, it is easy to verify that $c(x) = 0$ and $b(x) = h'(x)$. Collecting the remaining equations, the boundary layer approximation can be reduced to the following equations for the expansion coefficients:

$$h' = \frac{60}{7xh^3}\left(1 - \frac{9}{5}h^2a\right), \tag{20}$$

$$a' = \frac{2}{x}a + \frac{30x}{7h^3}\left(1 - \frac{3}{h^2a}\right). \tag{21}$$

Now it is easy to see that $a \to 0$ leads to a square root singularity because of the $1/a$ term in the last equation. If the location of the singularity does not depend too much on initial conditions, the scaling of the separation point, and thus, for r_j will follow from Eq. (16), which coincides with Eq. (3). It is a challenging task, on which we are currently working, to generalize this approach to be able to pass through the separation point and to describe the flow structures that we observe.

6. Conclusion

We have shown, that for low Reynolds number, the circular hydraulic jump has different regimes, depending on the downstream fluid depth. These include a time-dependent flow, breaking the rotational symmetry. However, for low outer depth, the flow is laminar, and shows a transition from a state with separation only at the bottom to a state where there is a roller at the free surface, and thus two separation points. The flow in the latter case is analogous to that of a broken surface wave. The

separation point at the bottom tends to be located at the same spot, irrespective of the type of flow. Furthermore, the surface velocities decrease linearly before the jump, and as $1/r$ after the jump, in both situations. Our numerical simulations predict the same flow structures as observed, and thus confirms that a transition is taking place.

Acknowledgements

This work has been supported by the Danish National Research Council. TB acknowledges support from Novo-Nordisk fonden.

References

[1] Lord Rayleigh, Proc. Roy. Soc. London A 90 (1914).
[2] E. Watson J. Fluid Mech 20 (1964) 481.
[3] I. Tani, J. Phys. Soc. Japan 4 (1949) 212.
[4] A. Craik, R. Latham, R. Fawkes and P. Gribbon, J. Fluid. Mech. 112 (1981) 347.
[5] T. Bohr, P. Dimon and V. Putkaradze, J. Fluid. Mech. 254 (1993) 635.
[6] F. Higuera, J. Fluid. Mech 274 (1994) 69.
[7] R. Bowles and F. Smith, J. Fluid. Mech. 242 (1992) 145.
[8] C.M. Lemos, Wave Breaking a Numerical Study (Berlin, Springer, 1992).
[9] S. Goldstein, Q.J. Mech. Appl. Math. 1 (1948) 43.